

## Supporting Information:

### Enhancing Thermoelectric Performance of $\text{Sn}_{0.5}\text{Ge}_{0.5}\text{Te}$ via Doping with Sb/Bi and Alloying with $\text{Cu}_2\text{Te}$ . Optimization of Transport Properties and Thermal Conductivity.

Shaochang Song<sup>a</sup>, Chun-Wan Timothy Lo<sup>a</sup>, Masoud Aminzare<sup>a</sup>, Yu-Chih Tseng<sup>b</sup> and Suneesh Meledath Valiyaveetil<sup>d</sup>, Yuriy Mozharivskiy,<sup>\*a</sup>

<sup>a</sup> Department of Chemistry and Chemical Biology, McMaster University, Hamilton, Ontario, Canada.

<sup>b</sup> CanmetMATERIALS, Natural Resources Canada, Hamilton, Ontario, Canada.

<sup>c</sup> Institute of Atomic and Molecular Sciences, Academia Sinica, Taipei 10617, Taiwan

<sup>d</sup> Department of Physics, National Central University, Taoyuan City 32001, Taiwan.

† Corresponding author. Tel: +1-905-525-9140 x 27796; fax: +1-905-521-2773. E-mail: [mozhar@mcmaster.ca](mailto:mozhar@mcmaster.ca) (Y.Mozharivskiy).

### Expanded view of the X-ray powder diffraction patterns.

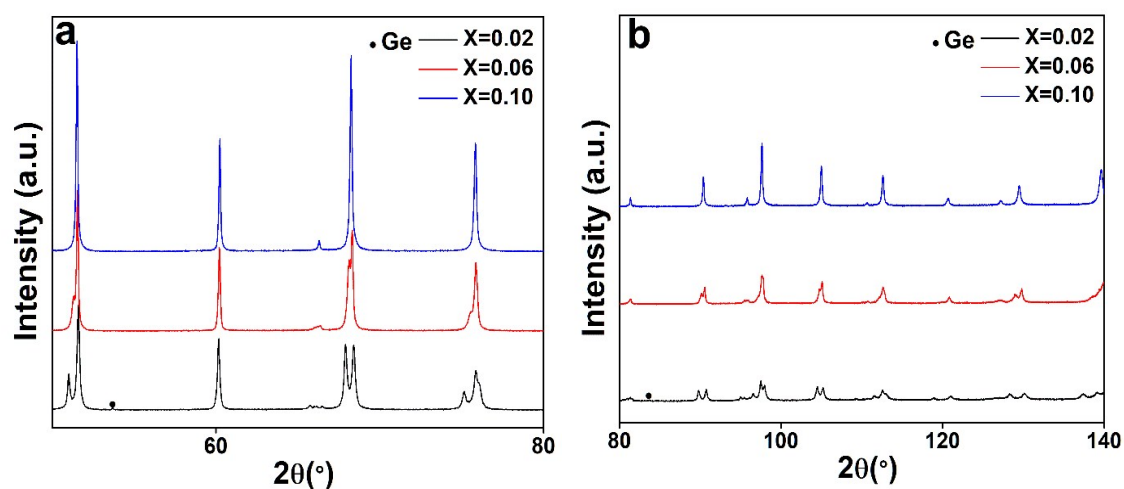


**Fig. S1:** Powder X-ray diffraction patterns of  $(\text{Sn}_{0.5}\text{Ge}_{0.5})_{1-1.5x}\text{Sb}_x\text{Te}$  in the (a) 40-80°, (b) 80-140°  $2\theta$  range at room temperature. The peak splitting is representative of the rhombohedral symmetry.

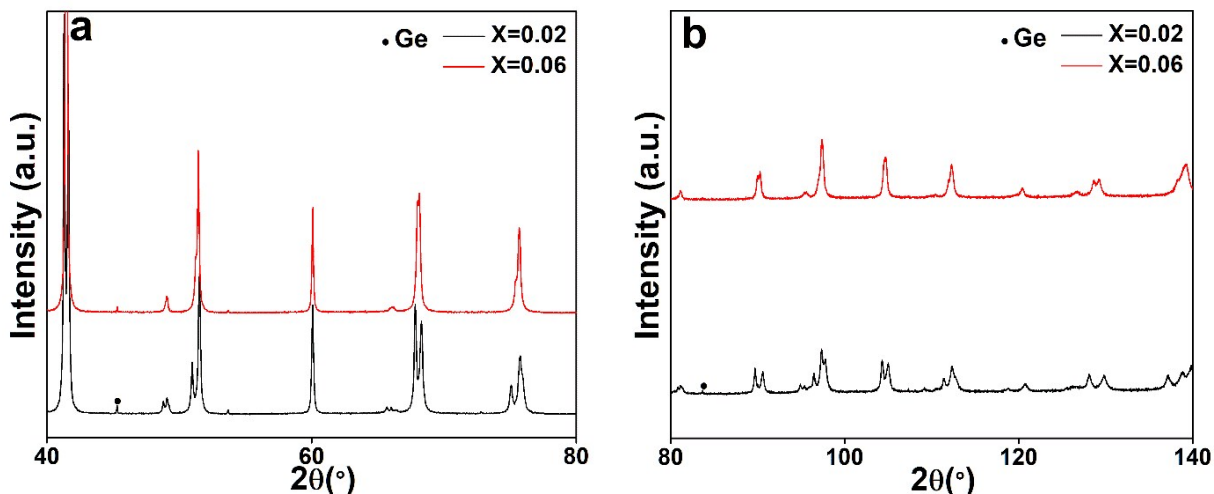


**Fig. S2:** Powder X-ray diffraction patterns of  $(\text{Sn}_{0.5}\text{Ge}_{0.5})_{1-1.5x}\text{Bi}_x\text{Te}$  in the (a)  $40\text{-}80^\circ$ , (b)  $80\text{-}140^\circ$   $2\theta$  range at room temperature. The peak splitting is representative of the rhombohedral symmetry.

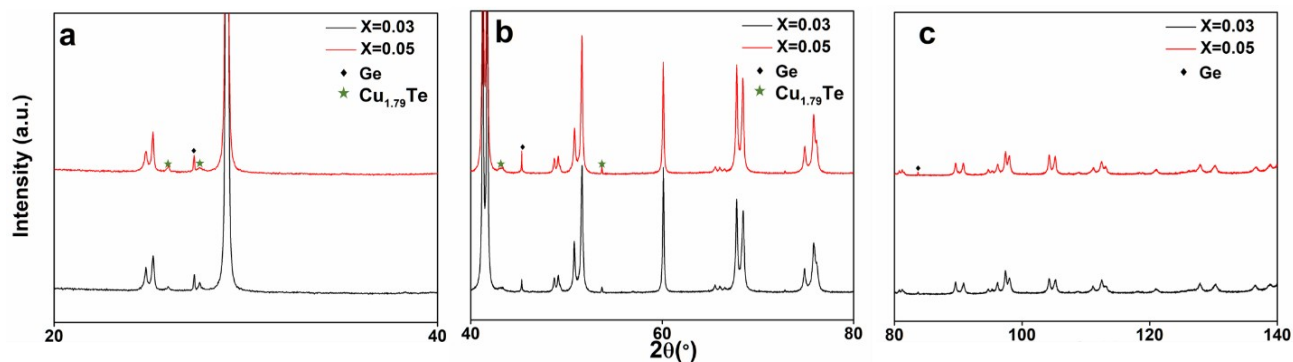


**Fig. S3:** Powder X-ray diffraction patterns of  $\text{Sn}_{0.5}\text{Ge}_{0.5}\text{Te}(\text{Cu}_2\text{Te})_x$  in the (a)  $20\text{-}40^\circ$ , (b)  $40\text{-}80^\circ$ , (c)  $80\text{-}140^\circ$   $2\theta$  range at room temperature. The peak splitting is representative of the rhombohedral symmetry.

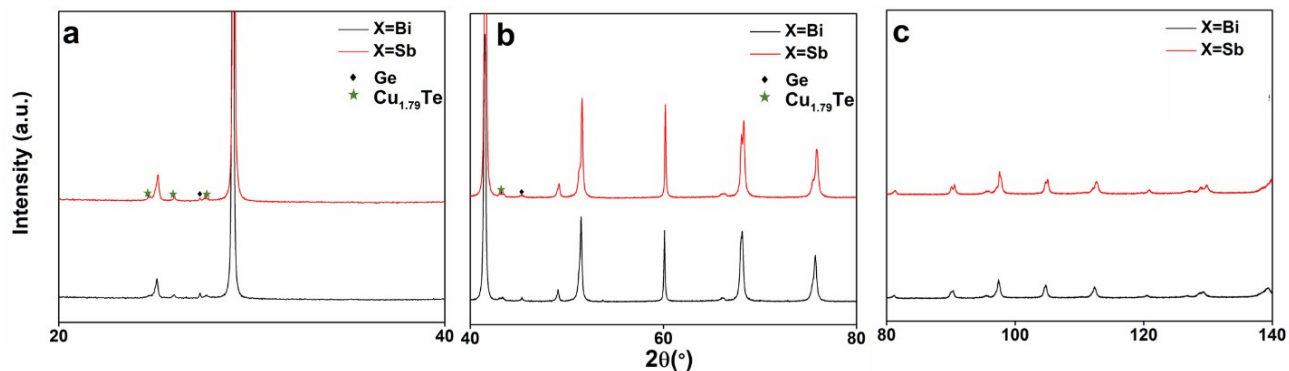


**Fig. S4:** Powder X-ray diffraction patterns of  $((\text{Sn}_{0.5}\text{Ge}_{0.5})_{0.91}\text{X}_{0.06}\text{Te}(\text{Cu}_2\text{Te})_{0.05}$  in the (a)  $20\text{-}40^\circ$ , (b)  $40\text{-}80^\circ$ , (c)  $80\text{-}140^\circ$   $2\theta$  range at room temperature. The peak splitting is representative of the rhombohedral symmetry. The peak splitting in the  $(\text{Sn}_{0.5}\text{Ge}_{0.5})_{0.91}\text{Bi}_{0.06}\text{Te}(\text{Cu}_2\text{Te})_{0.05}$  sample is small but still present.

## Scanning Electron Microscopy-Energy Dispersive X-ray Spectroscopy (SEM-EDS)

Sample polished with the 800 and 1200 grit sand papers were attached to SEM sample holders using a double-sided carbon tape. The SEM images and EDS data were collected on a TESCAN VEGA II LSU scanning electron microscope (20 kV accelerating voltage) equipped with an X-MAX (80mm<sup>2</sup>) X-ray EDS spectrometer (Oxford Instruments). Pure nickel metal was used as a calibration standard during the EDS analysis.

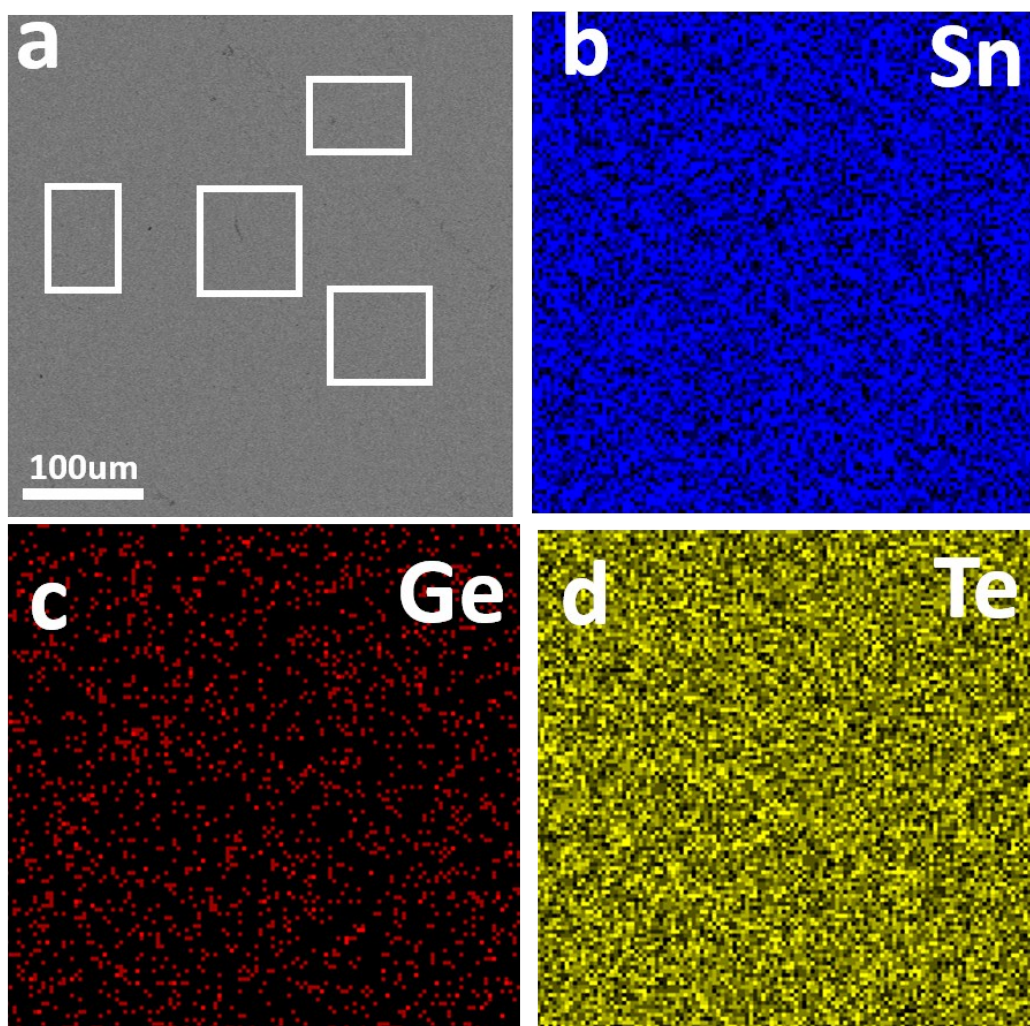


**Fig. S5:** (a) Back-scattered electron image; and (b-d) elemental mappings of Sn, Ge and Te of the  $\text{Sn}_{0.9}\text{Ge}_{0.1}\text{Te}$  sample. The average EDS composition of the selected areas in (a) is 46.3(3) at.% of Sn, 5.0(6) at.% of Ge, and 48.7(5) at.% of Te.

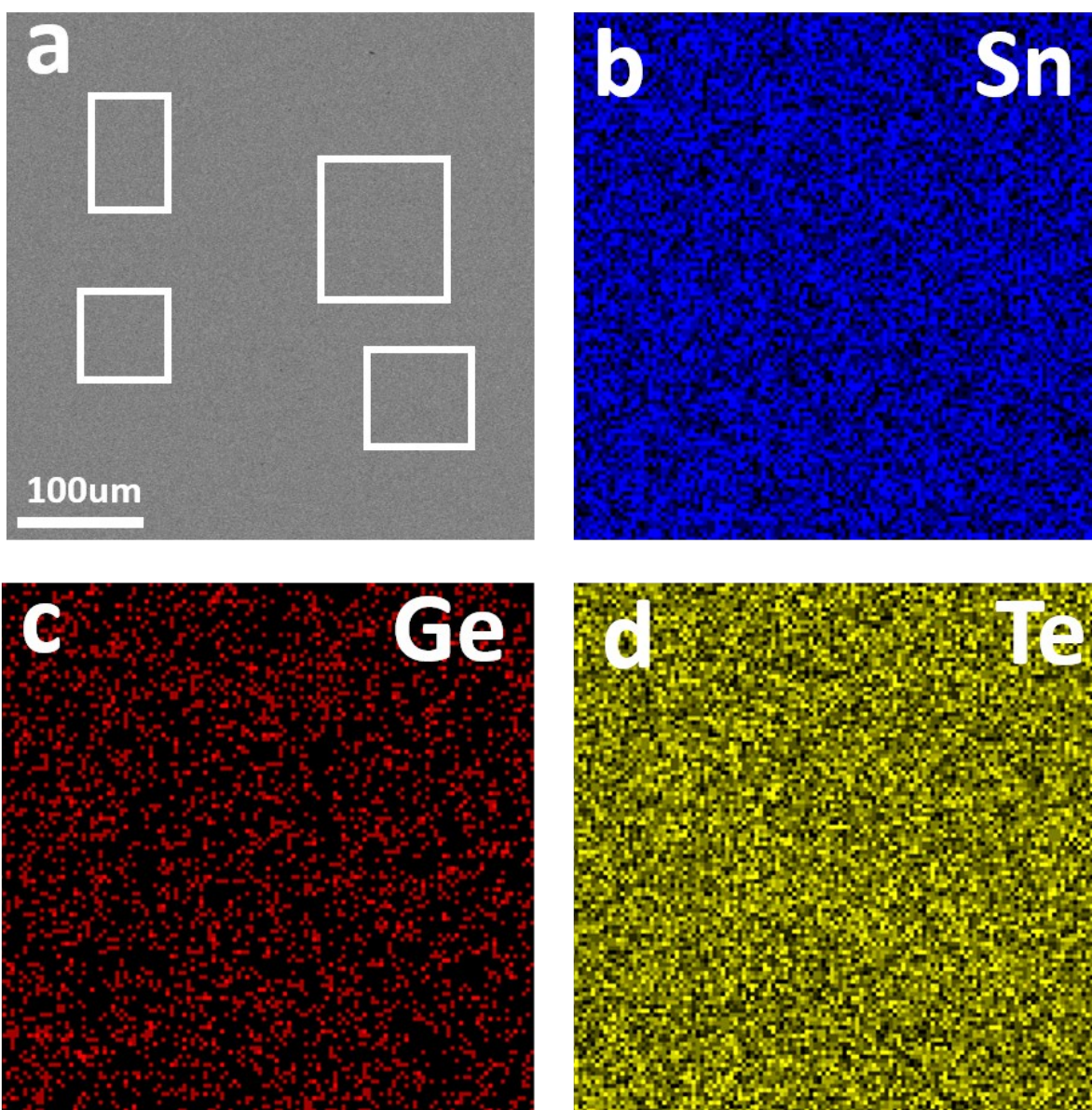


**Fig. S6:** (a) Back-scattered electron image; and (b-d) elemental mappings of Sn, Ge and Te of  $\text{Sn}_{0.7}\text{Ge}_{0.3}\text{Te}$ . The average EDS composition of the selected areas in (a) is 37.2(1) at.% of Sn, 14.2(4) at.% of Ge, and 48.6(2) at.% of Te.

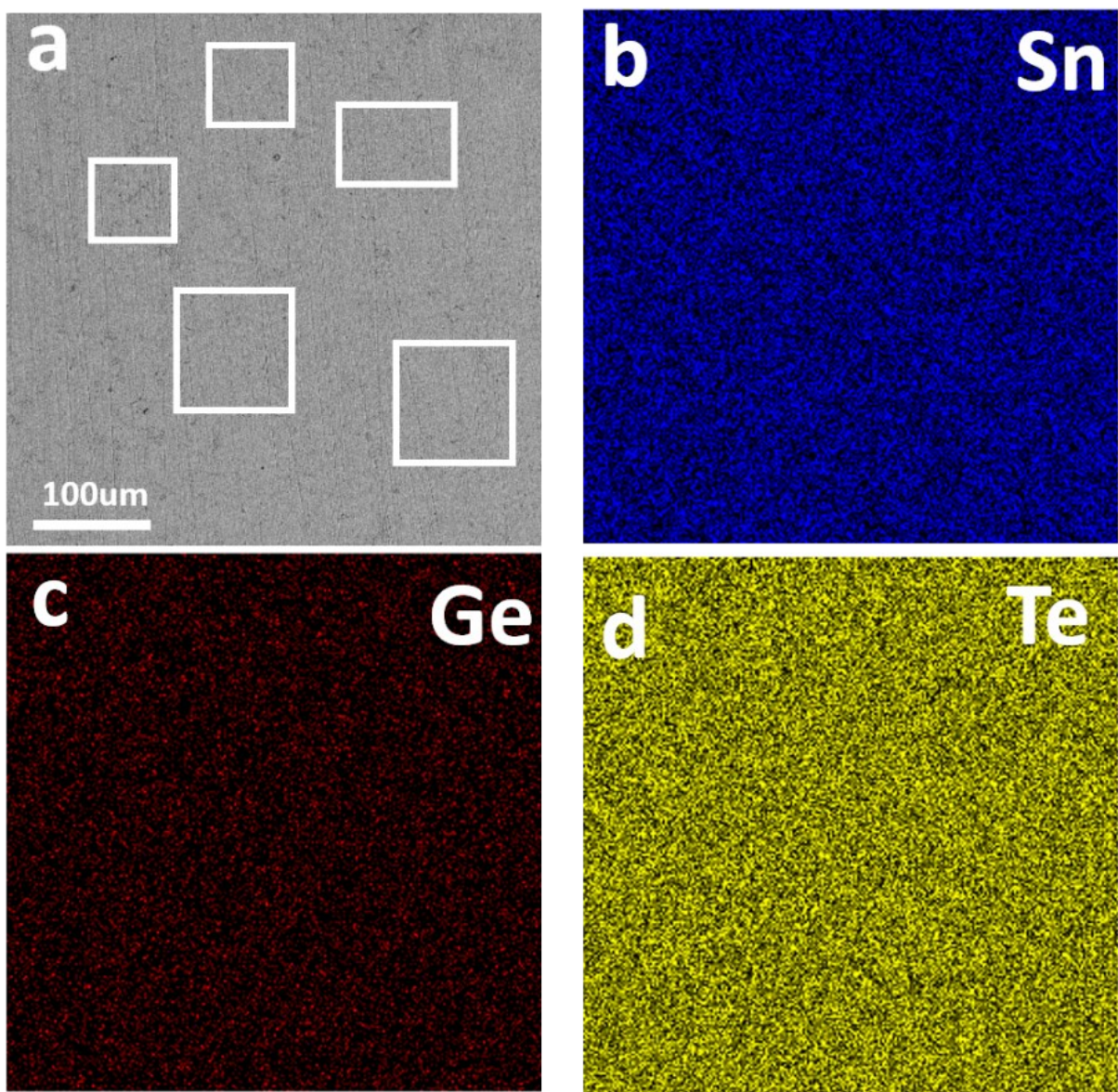


**Fig. S7:** (a) Back-scattered electron image; and (b-d) elemental mappings of Sn, Ge and Te of  $\text{Sn}_{0.9}\text{Ge}_{0.1}\text{Te}$ . The average EDS composition of the selected areas in (a) is 25.9(1) at.% of Sn, 25.1(2) at.% of Ge, and 49.0(2) at.% of Te.

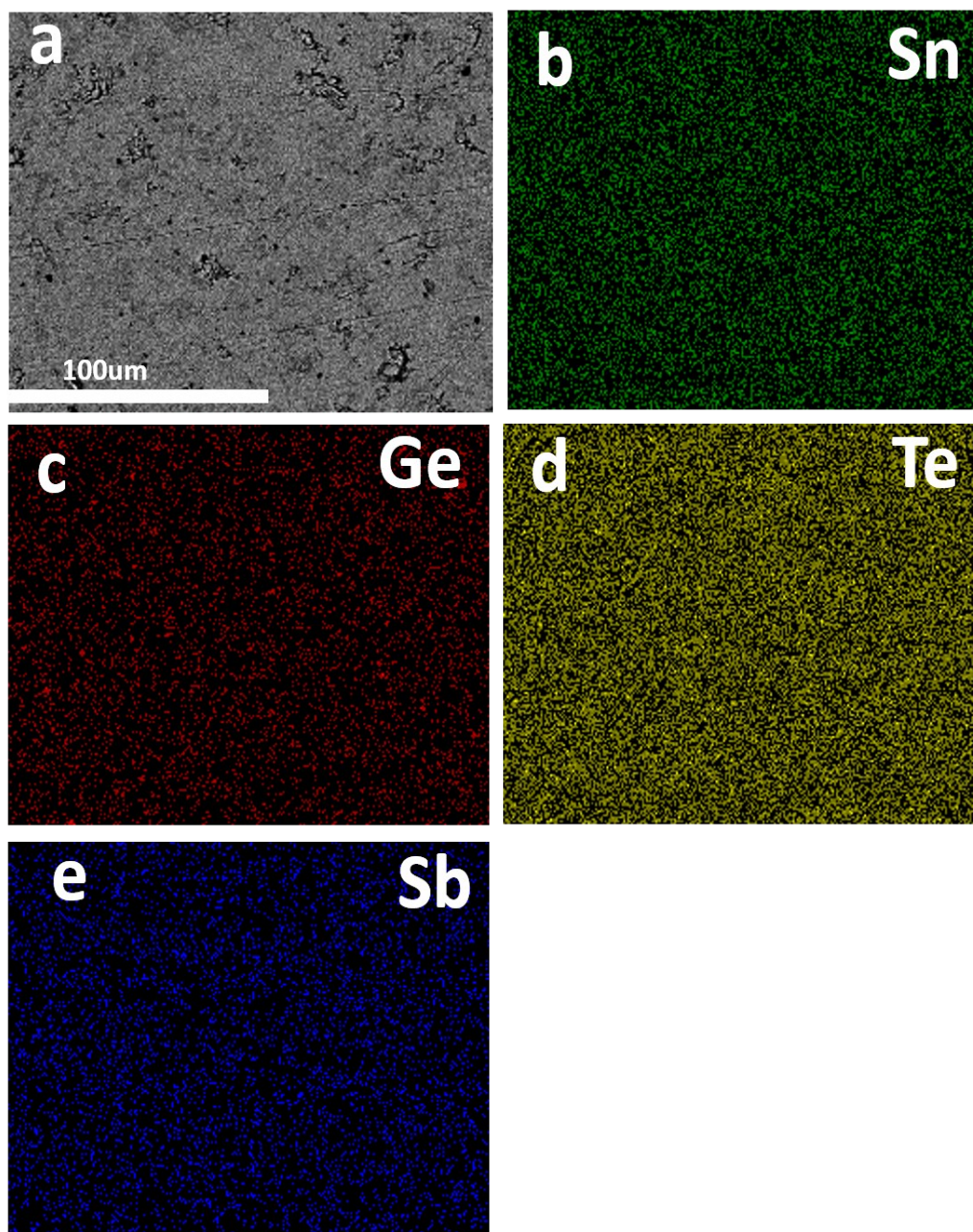


**Fig. S8:** (a) Back-scattered electron image; and (b-e) elemental mappings of Sn, Ge, Te and Sb of the  $(\text{Sn}_{0.5}\text{Ge}_{0.5})_{0.97}\text{Sb}_{0.02}\text{Te}$  sample. Due to the low doping levels of Sb and proximity of the  $k\alpha$  line of Sb (25.36 Å) to those of Sn (25.27 Å) and Te (27.47 Å), we could not reliably establish the concentration of Sb in the  $(\text{Sn}_{0.5}\text{Ge}_{0.5})_{0.97}\text{Sb}_{0.02}\text{Te}$  sample.

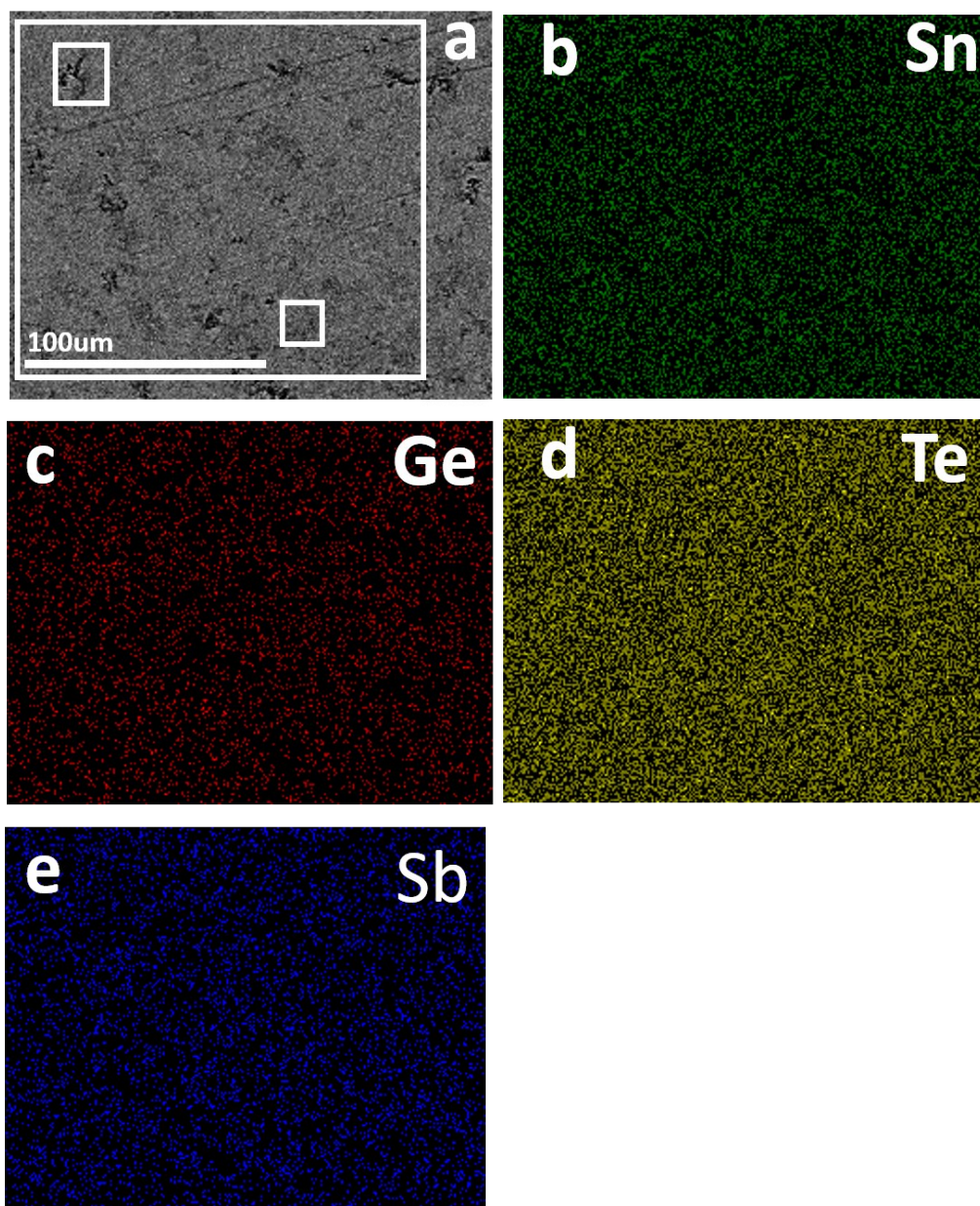


**Fig. S9:** (a) Back-scattered electron image; and (b-e) elemental mappings of Sn, Ge, Te and Sb of  $(\text{Sn}_{0.5}\text{Ge}_{0.5})_{0.91}\text{Sb}_{0.06}\text{Te}$ . EDS analysis of the selected areas in (a) yielded Sn, Ge, Te and Sb with the average amounts of 23.2(9), 22.9(6), 50.7(7) and 3.2(3) at. %, respectively.

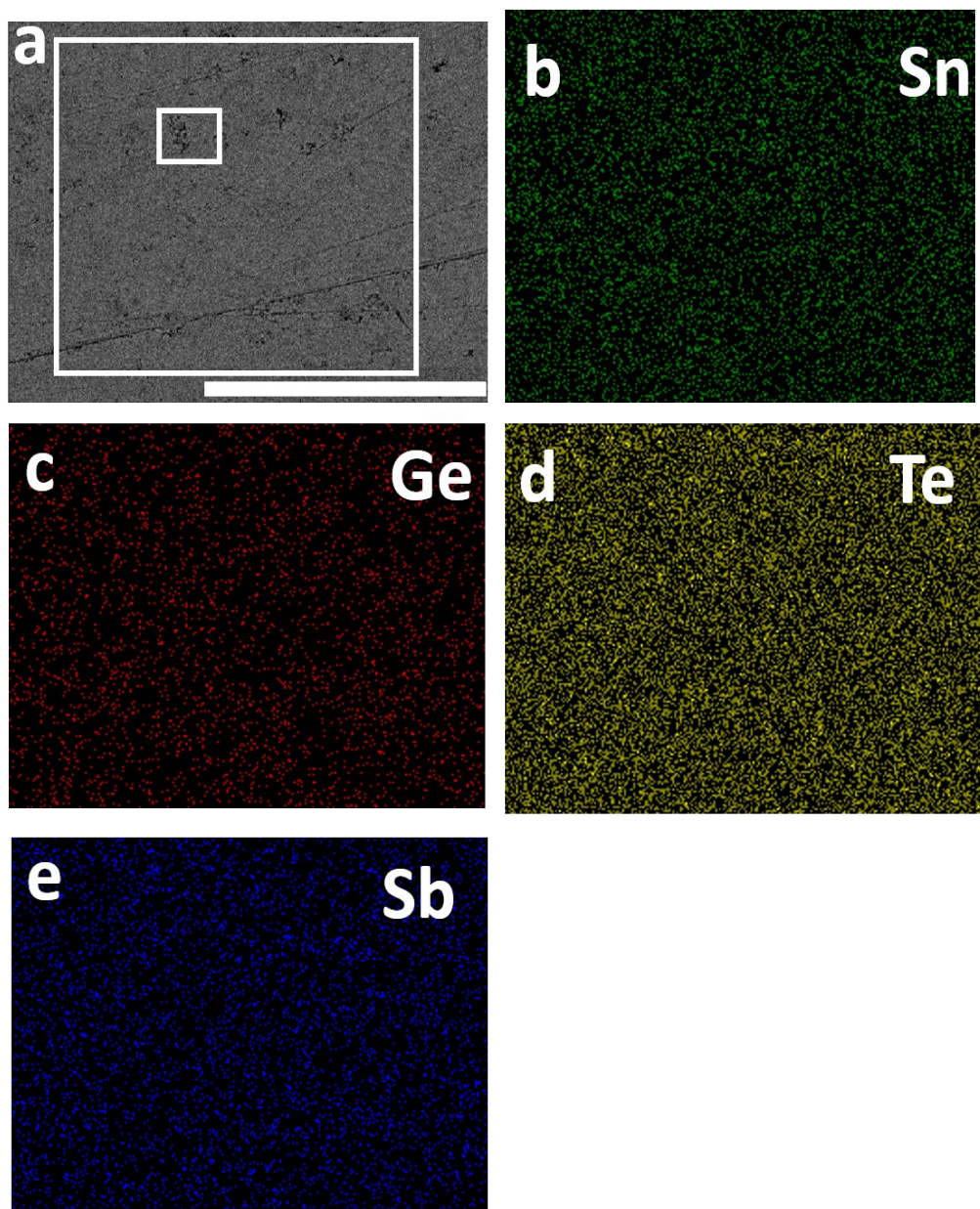


**Fig. S10:**(a) Back-scattered electron image; and (b-e) elemental mappings of Sn, Ge, Te and Sb of  $(\text{Sn}_{0.5}\text{Ge}_{0.5})_{0.85}\text{Sb}_{0.1}\text{Te}$ . EDS analysis of the selected areas in (a) yielded Sn, Ge, Te and Sb with the average amounts of 23.3(1), 21.0(1), 50.1(1) and 5.6(1) at. %, respectively.

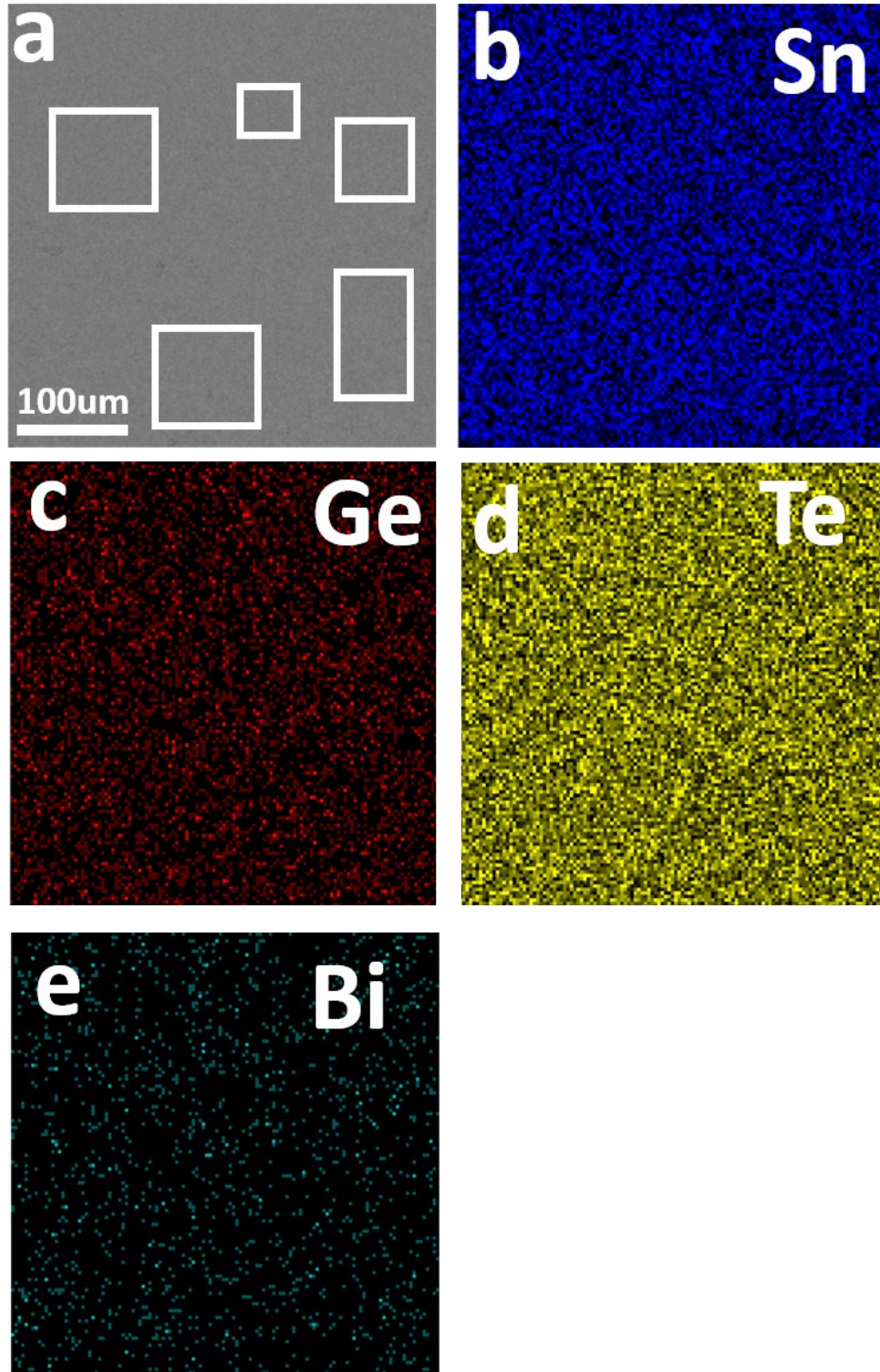


**Fig. S11:**(a) Back-scattered electron image; and (b-e) elemental mappings of Sn, Ge, Te and Bi of  $(\text{Sn}_{0.5}\text{Ge}_{0.5})_{0.97}\text{Bi}_{0.02}\text{Te}$ . EDS analysis of the selected areas in (a) yielded Sn, Ge, Te and Bi with the average amounts of 25.2(1), 24.6(4), 49.1(3) and 1.1(2) at. %, respectively.

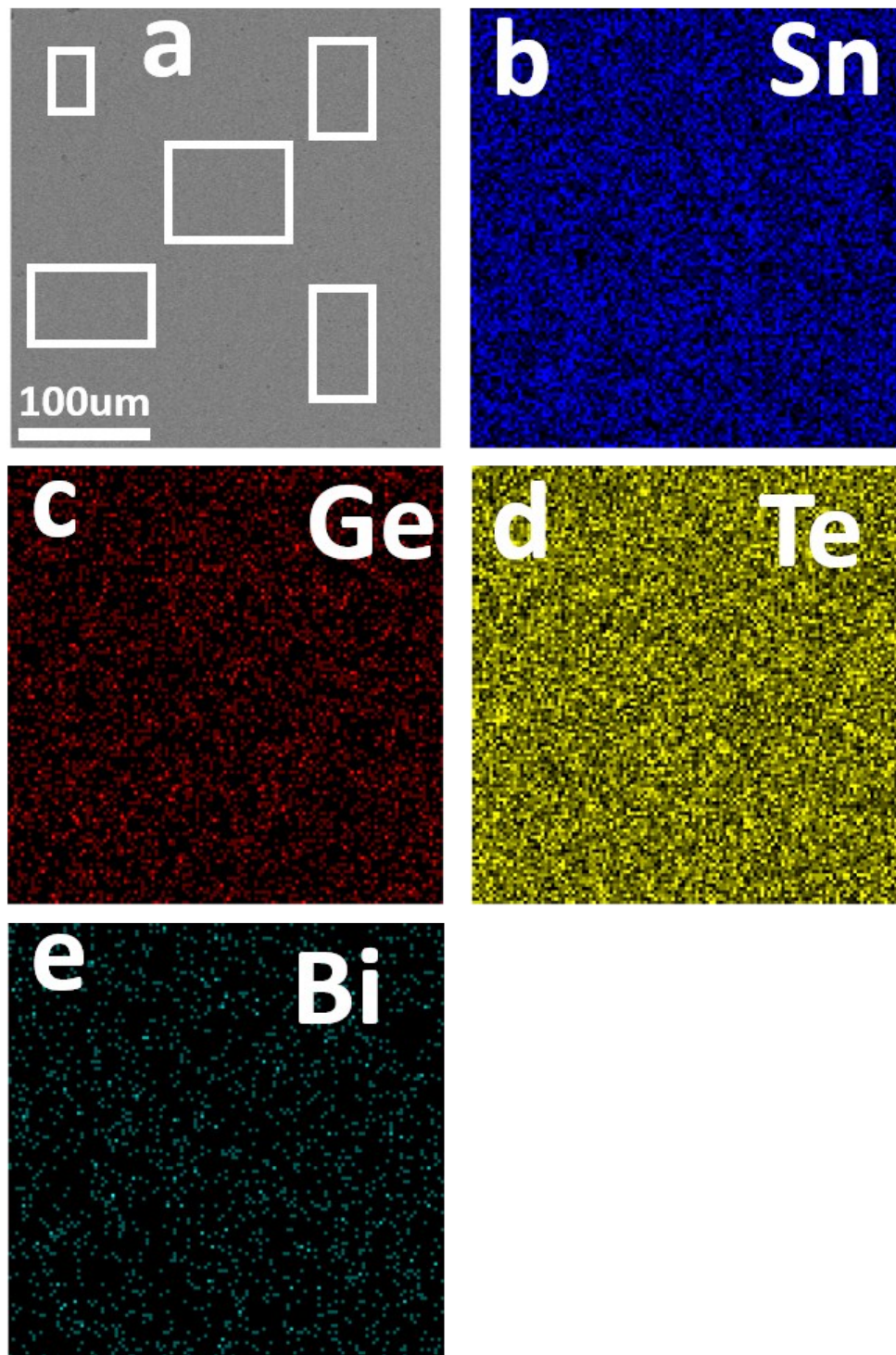


**Fig. S12:**(a) Back-scattered electron image; and (b-e) elemental mappings of Sn, Ge, Te and Bi of  $(\text{Sn}_{0.5}\text{Ge}_{0.5})_{0.91}\text{Bi}_{0.06}\text{Te}$ . The EDS analysis of the selected areas in (a) yielded Sn, Ge, Te and Bi with average amounts of 24.3(3), 23.3(3), 49.3(4) and 3.1(2) at. %, respectively.

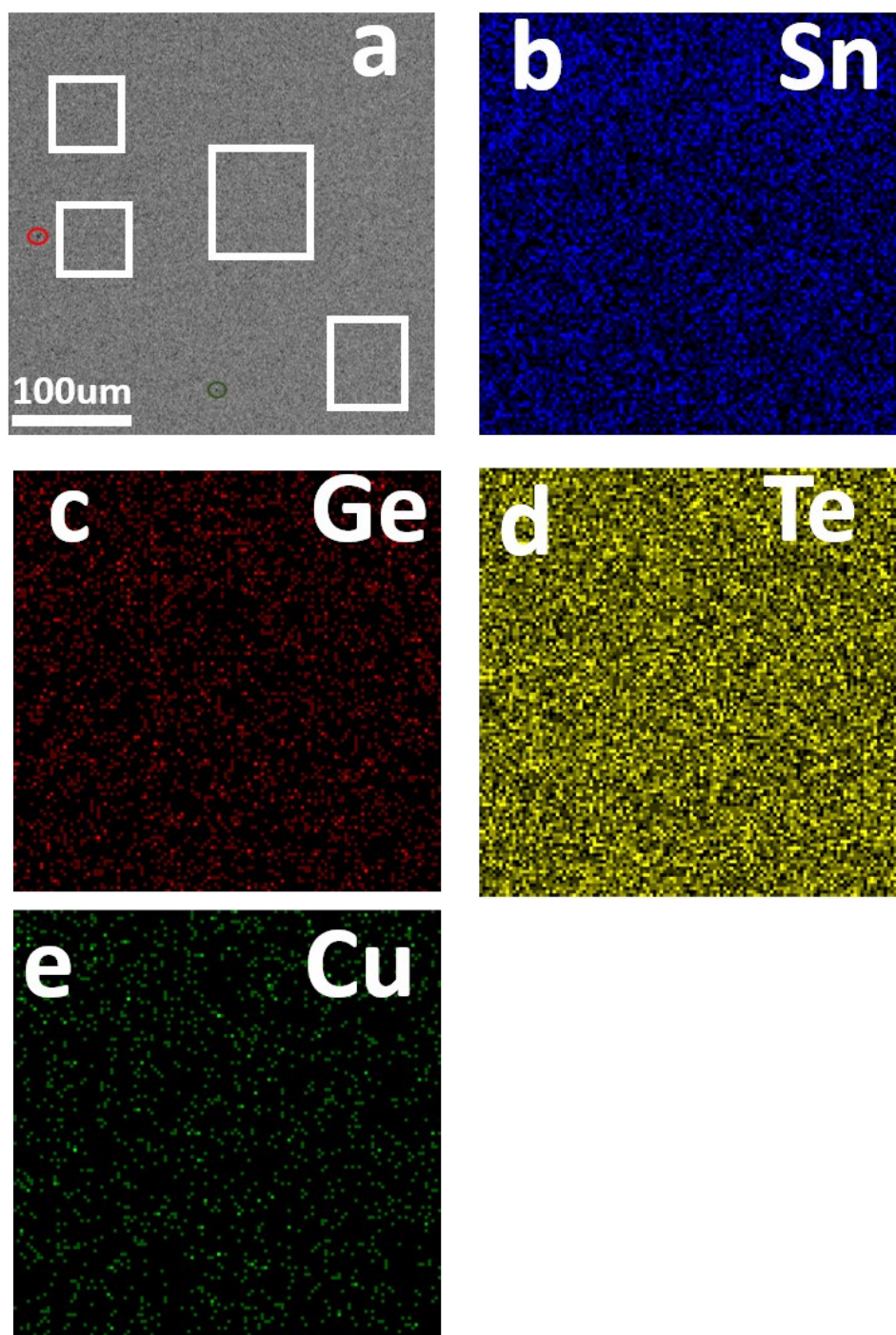


**Fig. S13:**(a) Back-scattered electron image,  $\text{Cu}_{1.8}\text{Te}$  as a secondary phase that gray spots in green circle, Ge as a tertiary phase that black spots in red circle; and (b-e) elemental mappings of Sn, Ge, Te and Cu of  $\text{Sn}_{0.5}\text{Ge}_{0.5}\text{Te}(\text{Cu}_2\text{Te})_{0.03}$ . The EDS analysis of the selected areas in (a) yielded Sn, Ge, Te and Cu with average amounts of 24.9(6), 23.9(3), 48.3(4) and 2.9(3) at. %, respectively.

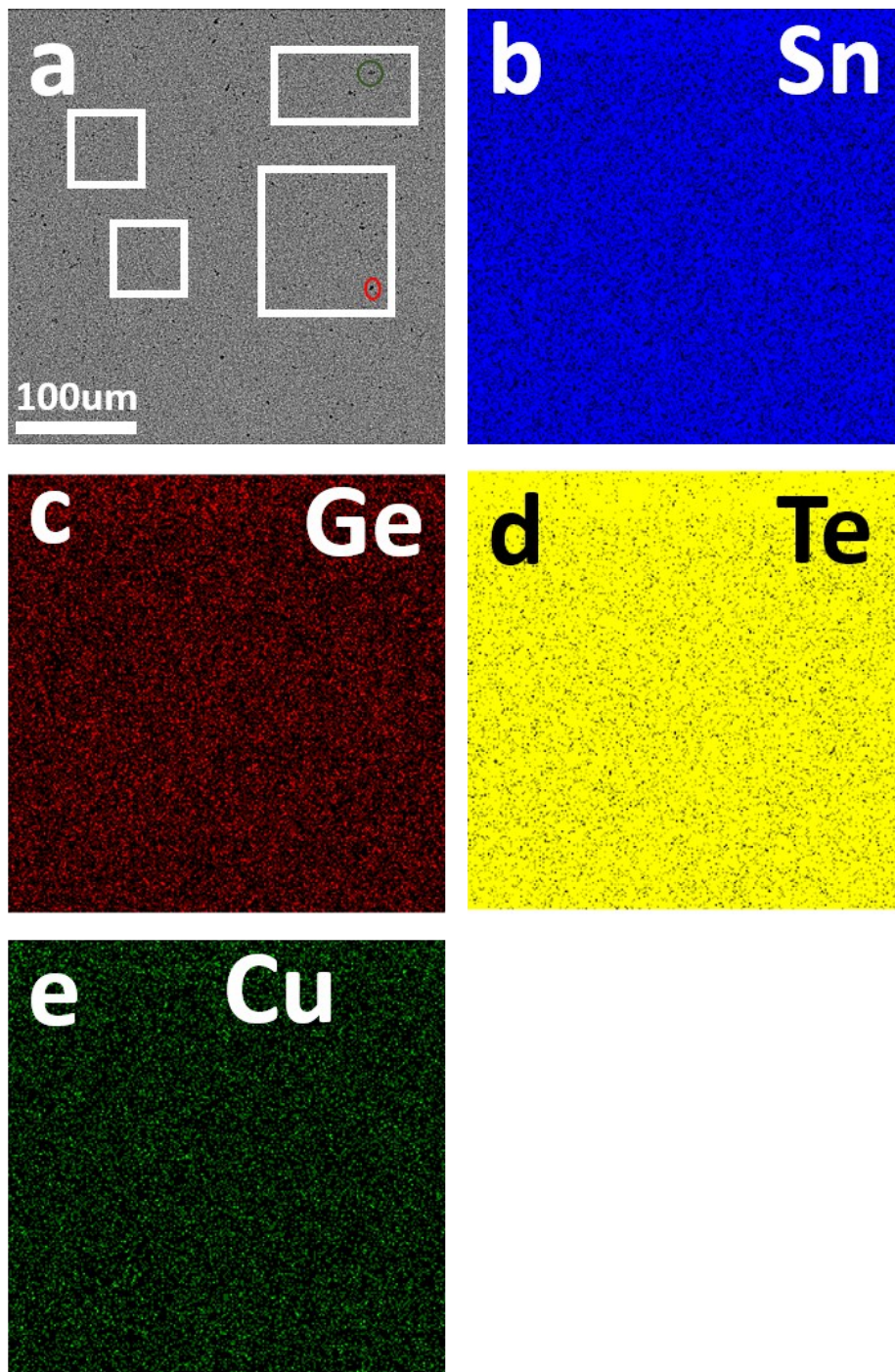


**Fig. S14:**(a) Back-scattered electron image of the  $\text{Sn}_{0.5}\text{Ge}_{0.5}\text{Te}(\text{Cu}_2\text{Te})_{0.05}$  sample. The  $\text{Cu}_{1.8}\text{Te}$  (inside the green circle) and Ge (a black dot inside the red circle) impurities are highlighted. (b-e) Elemental mappings of Sn, Ge, Te and Cu. EDS analysis of the selected areas in (a) yielded Sn, Ge, Te and Cu with the average amounts of 24.2(3), 23.4(4), 47.6(2) and 4.8(1) at. %, respectively.

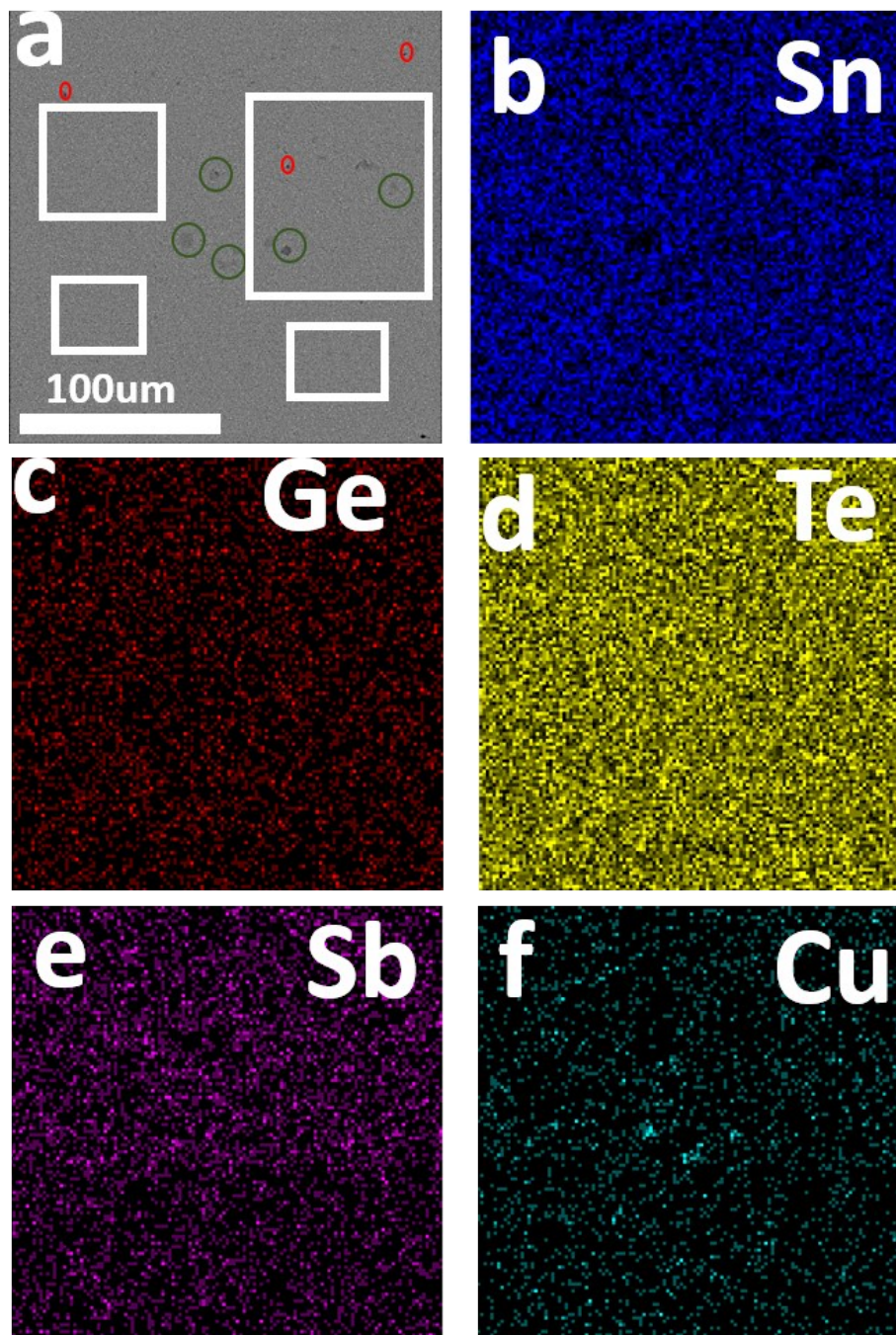


**Fig. S15:** (a) Back-scattered electron image of the  $(\text{Sn}_{0.5}\text{Ge}_{0.5})_{0.91}\text{Sb}_{0.06}\text{Te}(\text{Cu}_2\text{Te})_{0.05}$  sample. The  $\text{Cu}_{1.8}\text{Te}$  (dark gray dots inside the green circles) and Ge (black dots inside the red circles) impurities are highlighted. (b-f) Elemental mappings of Sn, Ge, Te, Sb and Cu. EDS analysis of the selected area in (a) yielded Sn, Ge, Te, Sb and Cu with the average amounts of 22.1(5), 21.4(5), 49.3(5), 2.8(4) and 4.4(8) at. %, respectively.

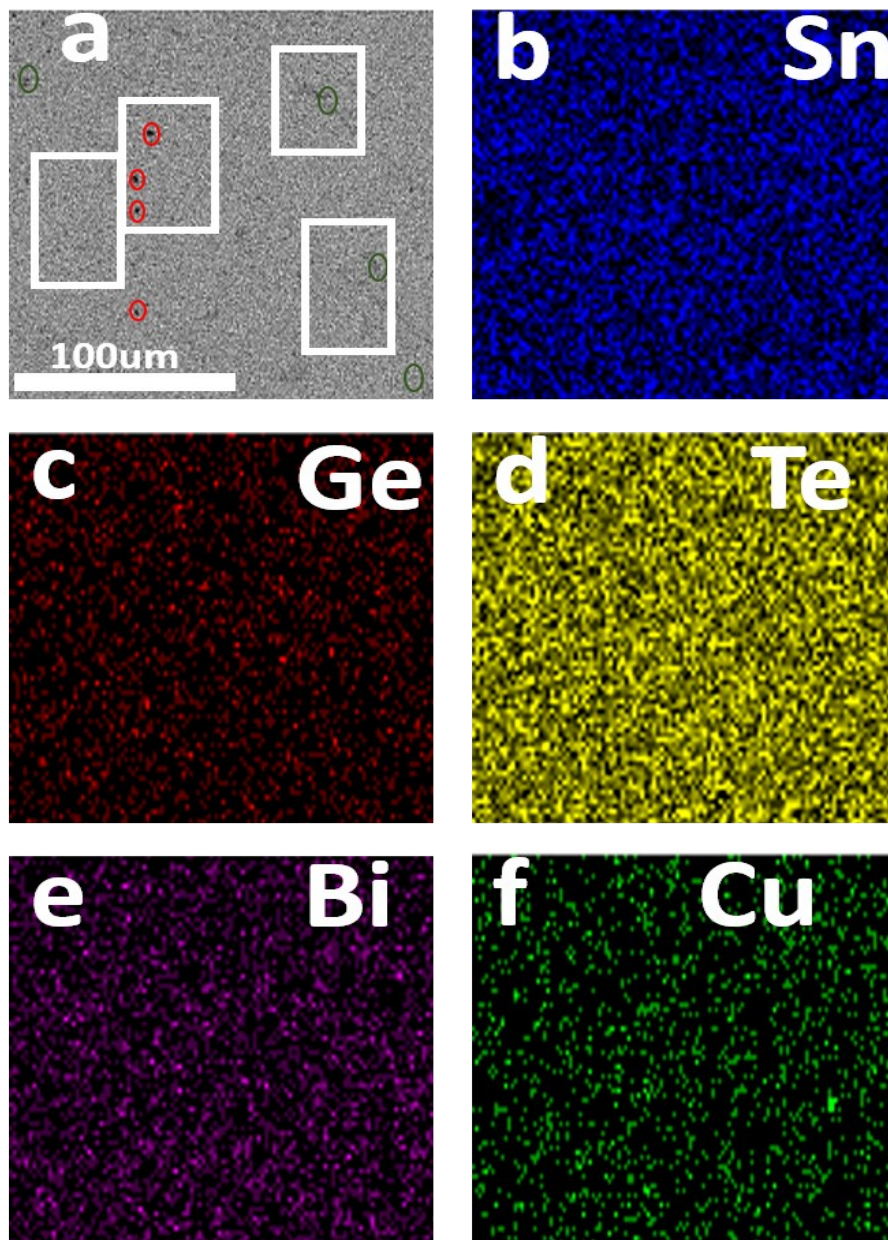


**Fig. S16:** (a) Back-scattered electron image of the  $(\text{Sn}_{0.5}\text{Ge}_{0.5})_{0.91}\text{Bi}_{0.06}\text{Te}(\text{Cu}_2\text{Te})_{0.05}$  sample. The  $\text{Cu}_{1.8}\text{Te}$  (dark gray dots inside the green circles) and Ge (black dots inside the red circles) impurities are highlighted. (b-f) elemental mappings of Sn, Ge, Te, Bi and Cu. EDS analysis of the selected area in (a) yielded Sn, Ge, Te, Bi and Cu with the average amounts of 22.6(6), 21.2(2), 49.0(3), 2.9(3) and 4.3(6) at. %, respectively.